MIT Open Access Articles

Study of forward Z + jet production in pp collisions at √s = 7 TeV

JHEP01(2014)033

Study of forward Z + jet production in pp collisions at $\sqrt{s} = 7$ TeV

The LHCb collaboration

E-mail: barter@hep.phy.cam.ac.uk

ABSTRACT: A measurement of the $Z(\to \mu^+\mu^-)$+jet production cross-section in *pp* collisions at a centre-of-mass energy $\sqrt{s} = 7$ TeV is presented. The analysis is based on an integrated luminosity of $1.0\,\text{fb}^{-1}$ recorded by the LHCb experiment. Results are shown with two jet transverse momentum thresholds, 10 and 20 GeV, for both the overall cross-section within the fiducial volume, and for six differential cross-section measurements. The fiducial volume requires that both the jet and the muons from the Z boson decay are produced in the forward direction ($2.0 < \eta < 4.5$). The results show good agreement with theoretical predictions at the second-order expansion in the coupling of the strong interaction.

doi:10.1007/JHEP01(2014)033

Contents

1 Introduction

Measurements of electroweak boson production in the forward region are sensitive to parton distribution functions (PDFs) at low Bjorken-x which are not particularly well constrained by previous results [1]. The LHCb experiment has recently presented measurements of inclusive W and Z boson[1] production in the muon decay channels [2] and inclusive Z boson production in the electron [3] and the tau lepton [4] decay channels. This article presents a measurement of the inclusive Z+jet production cross-section in proton-proton collisions at LHCb. These interactions typically involve the collision of a sea quark or gluon with a valence quark, and measurements of Z boson production in association with jets are sensitive to the gluon content of the proton [5]. LHCb is sensitive to a region of phase space in which both the Z boson and the jet are produced in the forward region. Measurements at LHCb are therefore complementary to those at ATLAS [6] and CMS [7, 8]. Hence, measurements of the Z+jet production cross-section at LHCb enable comparisons of different PDF predictions and their relative performances in this previously unprobed region of phase space.

The Z+jet production cross-section, in addition to being sensitive to the PDFs at low Bjorken-x, is influenced by higher order contributions in perturbative quantum chromo-dynamics (pQCD). Studies of the Drell-Yan process in the forward region are sensitive to

---

[1]Throughout this article Z includes both the Z and the virtual photon (γ^*) contribution.

multiple radiation of partons [9]. Measurements in the forward region have not been used to tune generators and, consequently, studies of Z+jet production in the forward region can be used to test the accuracy of different models. Theoretical predictions for the Z+jet process are available at $\mathcal{O}(\alpha_s^2)$ [10–17], where α_s is the strong-interaction coupling strength. Similar analyses at ATLAS [6] and CMS [7, 8] have shown reasonable agreement between data and such predictions.

This measurement of the cross-section of Z $\to \mu^+\mu^-$ events with jets in the final state uses data corresponding to an integrated luminosity of $1.0\,\mathrm{fb}^{-1}$ taken by the LHCb experiment in pp collisions at a centre-of-mass energy of $7\,\mathrm{TeV}$. The analysis is performed in a fiducial region that closely corresponds to the kinematic coverage of the LHCb detector. For the dimuon decay of the Z boson, this requirement is the same as that in ref. [2]. Both final state muons are required to have a transverse momentum,[2] p_T^μ, greater than $20\,\mathrm{GeV}$, and to have pseudorapidity[3] in the range $2.0 < \eta^\mu < 4.5$. The invariant mass of the dimuon system is required to be in the range $60 < M_{\mu\mu} < 120\,\mathrm{GeV}$. Jets are reconstructed using the anti-k_T algorithm [18] with distance parameter $R = 0.5$, and are required to be in the fiducial region $2.0 < \eta^\mathrm{jet} < 4.5$, and to be separated from decay muons of the Z boson by $\Delta r(\mu, \mathrm{jet}) > 0.4$. This separation is defined such that $\Delta r^2 \equiv \Delta\phi^2 + \Delta\eta^2$, where $\Delta\phi$ is the difference in azimuthal angle and $\Delta\eta$ the difference in pseudorapidity between the muon and the jet directions. Results are presented for two thresholds of the jet transverse momentum: $p_\mathrm{T}^\mathrm{jet} > 20\,\mathrm{GeV}$ and $p_\mathrm{T}^\mathrm{jet} > 10\,\mathrm{GeV}$. Both the total Z+jet cross-section and the cross-section ratio of Z+jet production to inclusive Z production are reported. In addition, six differential cross-sections for Z+jet production are presented as a function of the Z boson rapidity and transverse momentum, the pseudorapidity and transverse momentum of the leading[4] jet, and the difference in azimuthal angle and in rapidity between the Z boson and this jet. These differential measurements are presented normalised to the total Z+jet cross-section. The data are compared to predictions at $\mathcal{O}(\alpha_s)$ and $\mathcal{O}(\alpha_s^2)$ using different PDF parametrisations.

The remainder of this article is organised as follows: section 2 describes the LHCb detector and the simulation samples used; section 3 provides an overview of jet reconstruction at LHCb; section 4 describes the selection and reconstruction of candidates and the determination of the background level; section 5 describes the cross-section measurement; the associated systematic uncertainties are discussed in section 6; the results are presented in section 7; section 8 concludes the article.

2 LHCb detector and simulation

The LHCb detector [19] is a single-arm forward spectrometer covering the pseudorapidity range $2 < \eta < 5$, designed for the study of particles containing b or c quarks. The detector includes a high-precision tracking system consisting of a silicon-strip vertex detector (the

---

[2]Throughout this article natural units, where $c = 1$, are used.

[3]The pseudorapidity is defined to be $\eta \equiv -\ln(\tan(\theta/2))$, where the polar angle θ is measured with respect to the beam axis. The rapidity of a particle is defined to be $y \equiv 0.5\ln[(E + p_z)/(E - p_z)]$, where the particle has energy E and momentum p_z in the direction of the beam axis.

[4]The leading jet is defined to be the highest transverse momentum jet in the fiducial region.

VELO) surrounding the pp interaction region, a large-area silicon-strip detector (the TT) located upstream of a dipole magnet with a bending power of about $4\,\mathrm{Tm}$, and three stations of silicon-strip detectors and straw drift tubes placed downstream. The combined tracking system provides a momentum measurement with relative uncertainty that varies from $0.4\,\%$ at $5\,\mathrm{GeV}$ to $0.6\,\%$ at $100\,\mathrm{GeV}$, and impact parameter resolution of $20\,\mu\mathrm{m}$ for tracks with large transverse momentum. Charged hadrons are identified using two ring-imaging Cherenkov detectors [20]. Photon, electron and hadron candidates are identified by a calorimeter system consisting of scintillating-pad (SPD) and preshower detectors, an electromagnetic calorimeter and a hadronic calorimeter. Muons are identified by a system composed of alternating layers of iron and multiwire proportional chambers [21]. The trigger [22] consists of a hardware stage, based on information from the calorimeter and muon systems, followed by a software stage, which applies a full event reconstruction.

To avoid the possibility that a few events with high occupancy dominate the CPU time of the software trigger, a set of global event cuts (GEC) is applied on the hit multiplicities of most subdetectors used in the pattern recognition algorithms. The dominant GEC in the trigger selection used in this analysis is the requirement that the hit multiplicity in the SPD, n_{SPD}, is less than 600.

In the simulation, pp collisions are generated using PYTHIA 6.4 [23] with a specific LHCb configuration [24], with the CTEQ6ll [25] parametrisation for the PDFs. Decays of hadronic particles are described by EVTGEN [26], in which final state radiation is generated using PHOTOS [27]. The interaction of the generated particles with the detector and its response are implemented using the GEANT4 toolkit [28, 29] as described in ref. [30]. The main simulation sample used in this analysis is an $\mathcal{O}(\alpha_s)$ prediction of the Z+jet process, with the Z boson decaying to two muons. In addition, inclusive $Z \to \mu^+\mu^-$ events are generated at leading order in pQCD, where all jets are produced by the parton shower, in order to study various stages of the analysis with an independent simulation sample. This simulation sample is hereafter referred to as the inclusive Z sample.

3 Jet reconstruction

Inputs for jet reconstruction are selected using a particle flow algorithm. In order to benefit from the good momentum resolution of the LHCb tracking system, reconstructed tracks serve as charged particle inputs to the jet reconstruction. Tracks corresponding to the decay muons of the Z boson are excluded. The neutral particle inputs are derived from the energy deposits in the electromagnetic and hadronic calorimeters. If the deposits are matched to tracks, the expected calorimeter energies associated with the tracks are subtracted. The expected calorimeter energy is determined based on the likelihood that the track is associated with a charged hadron, a muon, or an electron, using information from the particle identification systems. If a significant energy deposit remains after the subtraction, the energy is associated with a neutral particle detected in the calorimeter. The use of the different particle identification hypotheses has negligible impact on the results presented in this article, since the jets studied here are mostly initiated by light quarks and gluons. Finally, in order to reduce the contribution from multiple proton-proton interactions, charged particles from tracks reconstructed within the VELO are not

considered if they are associated to a different primary vertex to that of the Z boson. The charged particles and energy clusters are reconstructed into jets using the anti-k_T algorithm [18], with distance parameter $R = 0.5$, as implemented in FASTJET [31].

The same jet reconstruction algorithm is run on simulated Z+jet events. The anti-k_T algorithm is also applied to these simulated events at the hadron-level using information that is available before the detector simulation is performed. The inputs for these 'true' jets are all stable final state particles, including neutrinos, from the same proton-proton interaction that produced the Z boson, that are not products of the Z boson decay.

The transverse momentum of a reconstructed jet is scaled so that it gives an unbiased estimate of the true jet transverse momentum. The scaling factor, typically between 0.9 and 1.1, is determined from simulation and depends on the jet pseudorapidity and transverse momentum, the fraction of the jet transverse momentum measured with the tracking systems, and the number of proton-proton interactions in the event. The energy resolution of reconstructed jets varies with the jet energy. The half width at half maximum for the distribution of $p_\mathrm{T}^\mathrm{reco}/p_\mathrm{T}^\mathrm{true}$ is typically 10-15 % for jets with transverse momenta between 10 and 100 GeV. In simulation, 90 % of jets with at least 10 GeV transverse momentum are reconstructed with $\Delta r < 0.13$ in $\eta - \phi$ space with respect to the true jet. At the p_T threshold of 20 GeV the corresponding radius is 0.08.

In order to reduce the number of spurious fake jets, and to select jets from the same interaction as that of the Z boson with a good estimate of the jet energy, additional jet identification requirements are imposed. Jets are required to contain at least two particles matched to the same primary vertex, to contain at least one track with $p_\mathrm{T} > 1.8$ GeV, and to contain no single particle with more than 75 % of the jet's transverse momentum.

4 Selection and event reconstruction

The Z $\rightarrow \mu^+\mu^-$ selection follows that described in ref. [2]. The events are initially selected by a trigger that requires the presence of at least one muon candidate with $p_\mathrm{T}^\mu > 10$ GeV. Selected events are required to contain two reconstructed muons with $p_\mathrm{T}^\mu > 20$ GeV and $2.0 < \eta^\mu < 4.5$, and one of these muons is required to have passed the trigger. The invariant mass of the dimuon pair must be in the range $60 < M_{\mu\mu} < 120$ GeV. The relative uncertainty on the measured momentum of each muon is required to be less than 10 % and the χ^2 probability for the associated track larger than 0.1 %. In total, 53 182 Z $\rightarrow \mu^+\mu^-$ candidates are selected.

A reconstructed jet with pseudorapidity in the range $2.0 < \eta^\mathrm{jet} < 4.5$ is also required in the selection. The separation between each of the decay muons of the reconstructed Z boson and the jet is required to be $\Delta r > 0.4$. Jets are reconstructed with transverse momentum above 7.5 GeV. Of the selected Z $\rightarrow \mu^+\mu^-$ candidates, 4 118 contain a reconstructed jet with transverse momentum above 20 GeV, and 10 576 contain a jet with transverse momentum above 10 GeV.

4.1 Background

The background contribution from random combinations of muons can come from semileptonic heavy flavour decays, W boson decays, or mesons that have decayed whilst passing

through the detector and have been reconstructed as muons, or hadrons that have passed through the calorimeters without interacting. This background is determined from the number of events containing two muons of the same charge that would otherwise pass the selection requirements. No significant difference is found using events where both muons have a positive charge or events where both muons have a negative charge. This background source contributes 5 ± 2 events for the $20\,\text{GeV}$ jet transverse momentum threshold and 16 ± 4 for the $10\,\text{GeV}$ threshold, where the uncertainties are statistical. The production of diboson pairs and heavy flavour decays of Z bosons, where the heavy flavour decay products decay to muons, are found to contribute negligible background levels to this analysis.

Decays from the $Z \rightarrow \tau^+\tau^-$ process where both tau leptons decay to muons and neutrinos are another potential background source. This background is determined from simulation, and contributes 7 ± 3 events for the $20\,\text{GeV}$ transverse momentum threshold, and 12 ± 3 events for the $10\,\text{GeV}$ threshold, where the uncertainties are statistical.

The background contribution from top quark pair production is also considered, where the top quark decay products include high transverse momentum muons. This background is determined from next-to-leading order (NLO) simulation to be 5 ± 2 events, where the uncertainties are statistical. This background is largely independent of the 10 and $20\,\text{GeV}$ jet transverse momentum thresholds as the top quark decays are associated with very high transverse momentum jets.

The background associated with events where a jet above a threshold is reconstructed, despite there being no true jet above that threshold, is treated as a migration. This background is corrected for by unfolding the transverse momentum distribution (see section 5).

The total background contribution for the $20\,\text{GeV}$ jet transverse momentum threshold is 17 ± 4 events, and the contribution for the $10\,\text{GeV}$ threshold is 33 ± 6 events. This corresponds to a sample purity $\rho \equiv S/(S + B)$, where S is the number of signal events and B is the number of background events, of $(99.6 \pm 0.1)\,\%$ for the $20\,\text{GeV}$ threshold and $(99.7 \pm 0.1)\,\%$ for the $10\,\text{GeV}$ threshold. These purities are consistent with that found in the inclusive Z boson analysis [2]. The purity shows no significant dependence on other kinematic variables of interest. Since the purity is high and has little variation with the transverse momentum threshold it is treated as constant for this analysis.

4.2 Z detection and reconstruction efficiencies

Following ref. [3], the total Z boson detection efficiency is factorised into four separate components as $\varepsilon_Z = \varepsilon_{\text{GEC}}\,\varepsilon_{\text{trigger}}\,\varepsilon_{\text{track}}\,\varepsilon_{\text{ID}}$, where the ε_X factors correspond to the efficiency associated with the GEC, the trigger requirements, the muon track reconstruction and the muon identification, respectively.

The GEC, applied in the trigger to stop very large events dominating processing time, cause signal events to be rejected. The associated inefficiency is obtained using the same method described in ref. [3], where an alternative dimuon trigger requirement[5] is used to

---

[5]This trigger route is not used elsewhere in this analysis as it has a lower efficiency than the single muon trigger.

determine the number of events that are rejected with $600 < n_{\text{SPD}} < 900$. The small number of events with $n_{\text{SPD}} > 900$ is found by extrapolation using a fit with a gamma function. This approach is applied to determine the efficiency as a function of the number of reconstructed primary vertices and the number of jets reconstructed in the event. The average efficiency is 91%.

The trigger efficiency for the single muon trigger is found using the same tag-and-probe method used in ref. [2]. Events in which at least one muon from the Z boson decay passed the trigger are selected. The fraction of events where the other muon from the Z boson decay fired the trigger determines the muon trigger efficiency. This efficiency is found to be independent of the number of jets reconstructed in the event and is determined as a function of the muon pseudorapidity. The efficiencies for the two muons are then combined to determine the efficiency with which at least one of the two muons in the decay passes the trigger, $\varepsilon_{\text{trigger}}(\eta_1, \eta_2) = \varepsilon(\eta_1) + \varepsilon(\eta_2) - \varepsilon(\eta_1)\varepsilon(\eta_2)$. This combination assumes that the probability that one muon fires the trigger is independent of whether the other muon fired the trigger. This is confirmed with simulated data. The average of this combined efficiency is approximately 96%.

The muon track reconstruction efficiency is determined using the tag-and-probe method, described in refs. [2] and [32]. Well reconstructed tracks in the muon stations are linked to hits in the TT detector in events containing one other high-purity muon candidate. The invariant mass of this dimuon pair is required to lie within $10\,\text{GeV}$ of the Z boson mass. The efficiency is determined as the fraction of events where the muon-station track is geometrically matched to a track in the tracking system that passes the track quality requirements. This efficiency depends on the muon pseudorapidity and the number of jets measured in the event, with an average efficiency of approximately 90% for each muon.

The muon identification efficiency is determined using the method described in ref. [2]. Events containing two tracks with an invariant mass within $5\,\text{GeV}$ of the Z boson mass are selected. One of the tracks is required to be identified as a muon. The fraction of events in which the other track is also identified as a muon defines the muon identification efficiency. This efficiency shows no dependence on the number of jets in the event and is found as a function of the muon pseudorapidity. The average muon identification efficiency is 99%.

4.3 Jet detection and reconstruction efficiencies

The jet detection efficiency is determined from simulation and is defined as the efficiency for a jet to be reconstructed with transverse momentum greater than $7.5\,\text{GeV}$, satisfying the jet selection criteria, given that a true jet is reconstructed in the same event. This efficiency is determined as a function of the true jet transverse momentum and shows little variation in the central region of the LHCb detector. Reweighting the simulation to have the same jet pseudorapidity distribution as data has a negligible effect on the efficiency. This efficiency is about 75% for jets with transverse momentum of about $10\,\text{GeV}$, but rises to about 96% for high transverse momentum jets, as shown in figure 1. The drop in efficiency at low transverse momentum is mainly due to the jet identification requirements having a larger effect in this region.
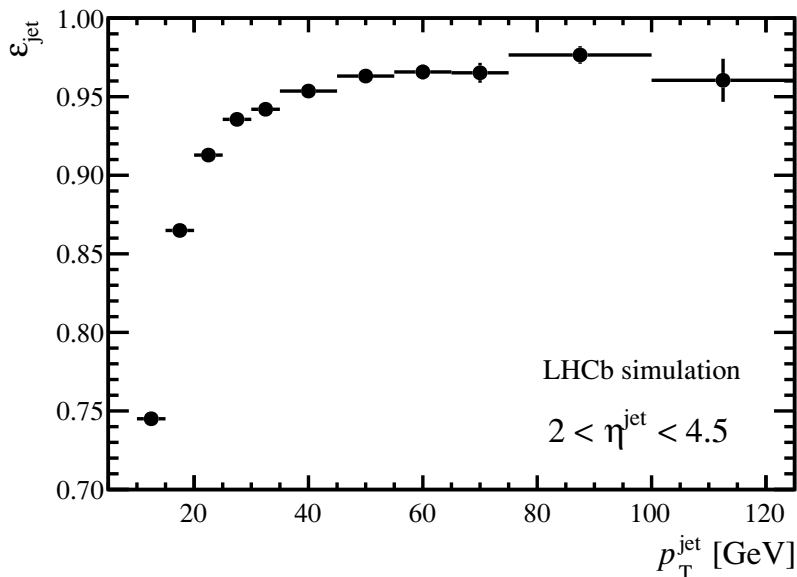
Figure 1. Jet identification efficiency as a function of the true jet p_T. The uncertainties shown are statistical. The zero on the vertical axis is suppressed.

5 Cross-section measurement

Events are selected with reconstructed jet transverse momentum above 7.5 GeV. Migrations in the jet transverse momentum distribution are corrected for by unfolding the distribution using the method of D'Agostini [33], as implemented in ROOUNFOLD [34]. Two iterations are chosen as this gives the best agreement between the unfolded distribution and the true distribution when the inclusive Z simulation sample is unfolded, using the same number of events in the inclusive Z simulation sample as are present in data. As a cross-check, the result is compared with the SVD unfolding method [35]. In these studies underflow bins are included in the unfolded distributions to account for the small number of events that lie below threshold after the unfolding procedure.

Each event is assigned a weight for the Z boson reconstruction, detection and selection efficiency, ε_Z. This enables the determination of the fraction of events within each bin of the unfolded jet transverse momentum, $N(p_T^{unf})$, corrected for the Z detection efficiency

$$N(p_T^{unf}) = \sum_{\text{events}} \frac{M(p_T^{unf}, p_T^{reco})}{\varepsilon_Z}, \tag{5.1}$$

where $M(p_T^{unf}, p_T^{reco})$ is the element of the matrix, obtained from the unfolding, that gives the probability that an event containing a jet with reconstructed transverse momentum in the bin p_T^{reco} contains a true jet with transverse momentum in the bin p_T^{unf}. For the differential distributions the matrix is determined for events restricted to the relevant bin in that differential distribution. This unfolding includes the correction for the background where a jet is reconstructed with p_T above the threshold despite there being no true jet above that threshold in the event.

Source	Relative uncertainty (%)
Unfolding	1.5
Z detection and reconstruction	3.5
Jet-energy scale, resolution and reconstruction	7.8
Final state radiation	0.2
Total excluding luminosity	8.6
Luminosity	3.5

Table 1. The relative uncertainty arising from each source of possible systematic uncertainties considered for the Z+jet cross-section for $p_T^{jet} > 20$ GeV. The relative uncertainties are similar for the 10 GeV threshold. The contributions from the different sources are combined in quadrature.

In order to measure the cross-section, a correction is applied to account for the jet reconstruction efficiency, ε_{jet}. The correction is performed for each bin in each differential distribution separately. In differential measurements an additional factor A_{mig} is applied to account for migration between different bins (for example, in the jet pseudorapidity distribution). These corrections are typically small $(2-3\%)$ and are taken from simulation. The cross-section is determined by dividing the resulting event yield, corrected for migrations and the reconstruction acceptance, by the integrated luminosity, $\int \mathcal{L} \, dt$, as follows

$$\sigma = \frac{\rho}{\int \mathcal{L} \, dt} \sum_{p_T^{\text{unf}} > p_T^{\text{thr}}} \frac{A_{\text{mig}}}{\varepsilon_{\text{jet}}} N(p_T^{\text{unf}}), \tag{5.2}$$

where p_T^{thr} is the relevant threshold, 20 or 10 GeV, and the sum is over the bins of the unfolded transverse momentum above this threshold. The purity of the sample, ρ, accounts for the presence of background as discussed in section 4.1. The luminosity is determined as described in ref. [36].

Measurements of the total Z+jet cross-section are quoted at the Born level in QED; the correction factors for final state radiation (FSR) of the muons are calculated with HERWIG++ [37]. Differential distributions are compared to theoretical predictions that include the effects of FSR, so they are not corrected for FSR from the muons. The differential distributions are also normalised to the total Z+jet cross-section above the relevant transverse momentum threshold, without corrections for FSR, so that their integral is unity.

6   Systematic uncertainties

The different contributions to the systematic uncertainty are discussed below and are summarised in table 1.

Two contributions associated with the unfolding are considered. The difference in the unfolded result between the SVD [35] and the D'Agostini [33] methods is assigned as an uncertainty. In addition, the unfolding process is carried out on the inclusive Z sample described in section 2 (which is an independent simulation sample to that used to perform the unfolding), and the difference between the unfolded distribution and the true distribution is assigned as a systematic uncertainty. The number of events considered in
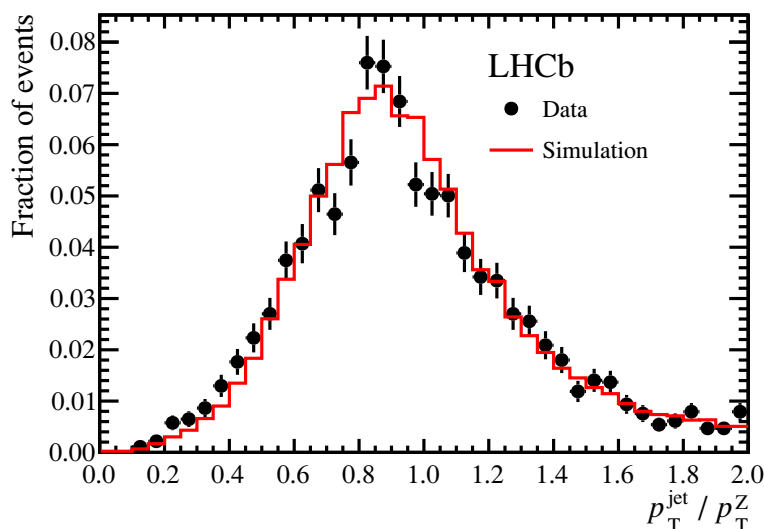
Figure 2. Comparison between data (black points) and simulation (red line) in the p_T^{jet}/p_T^Z distribution for selected Z+1-jet events where the Z boson and the jet are emitted azimuthally opposed. The uncertainties shown are statistical.

the independent sample is the same as the number in data. The differences between the results found using the D'Agostini method with one iteration and those found using two iterations are less than the uncertainties assigned from the unfolding method.

The systematic uncertainties for the muon identification and trigger efficiencies are obtained as in ref. [2], where the statistical uncertainties on the tag-and-probe method are used as systematic uncertainties on the efficiency. The systematic uncertainty associated with the GEC efficiency is considered as in ref. [3]. A variation in the fit model is applied and the change in efficiency is considered as a systematic uncertainty. In addition, the statistical uncertainty in the efficiency is assigned as a systematic uncertainty. The systematic uncertainty associated with the track reconstruction efficiency has two contributions. The uncertainty associated with the statistical precision of the efficiency determination is treated as in ref. [2]. By comparing the tag-and-probe method applied to simulation with the true efficiency, the method is found to be accurate to 0.3% for each muon. This sets the systematic uncertainty associated with the tag-and-probe method used to find the muon track reconstruction efficiency.

The systematic uncertainty associated with the jet identification requirements is determined by tightening these requirements and comparing the fraction of events rejected in data and simulation. These are found to agree at the level of about 3%. This is therefore used as a systematic uncertainty. The efficiency is cross-checked on the independent inclusive Z sample, and the difference is taken as an additional systematic uncertainty. The efficiency associated with the jet reconstruction, neglecting the jet identification requirements, is found to be about 98.5% at low transverse momentum, so an additional 1.5% uncertainty is assigned to this reconstruction efficiency component of ε_{jet} at low momentum. The jet-energy scale and resolution show no dependence on the separation of the Z

and the jet in the azimuthal angle. The jet-energy scale and resolution uncertainties associated with how well the detector response to jets is modelled in simulated data are therefore determined by selecting Z+1-jet events that are azimuthally opposed. In these events the Z boson and jet transverse momenta are expected to balance. Hence, the Z boson transverse momentum can be used as a proxy for the true jet transverse momentum. The $p_{\mathrm{T}}^{\mathrm{jet}}/p_{\mathrm{T}}^{\mathrm{Z}}$ distribution in the selected events is shown in figure 2, and is also considered as a function of the jet pseudorapidity and transverse momentum. The mean is found to agree between data and simulation at the level of about 3 %, consistent within the statistical precision. The width is consistent between data and simulation, and the resolution in simulation can be smeared at the level of about 10 % whilst maintaining this agreement. Based on these comparisons, systematic uncertainties to account for the reliability of the modelling are assigned to the jet-energy scale and resolution. In addition, a systematic uncertainty is assigned based on the difference in the jet-energy scale for gluon- and quark-initiated jets, and for the method used to correct the jet-energy scale. This contributes an additional 2 % systematic uncertainty on the jet-energy scale. These uncertainties are then propagated into the cross-sections and distributions measured. The contribution from the uncertainty on the jet-energy scale is the dominant uncertainty in most bins analysed.

The systematic uncertainty on the FSR correction applied to the total cross-section is determined by comparing the correction taken from HERWIG++ [37] and from PYTHIA [23] interfaced with PHOTOS [27], as found in ref. [2]. The difference in correction is at the level of 0.2 %.

The luminosity uncertainty is estimated to be 3.5 %, as detailed in ref. [36].

7 Results

The Z+jet cross-section and the cross-section ratio $\sigma(\mathrm{Z+jet})/\sigma(\mathrm{Z})$ are measured at the Born level. For the $p_{\mathrm{T}}^{\mathrm{jet}} > 20$ GeV threshold the results are

$$\sigma(\mathrm{Z+jet}) = 6.3 \pm 0.1\,(\mathrm{stat.}) \pm 0.5\,(\mathrm{syst.}) \pm 0.2\,(\mathrm{lumi.})\ \mathrm{pb},$$

$$\frac{\sigma(\mathrm{Z+jet})}{\sigma(\mathrm{Z})} = 0.083 \pm 0.001\,(\mathrm{stat.}) \pm 0.007\,(\mathrm{syst.}),$$

and for the $p_{\mathrm{T}}^{\mathrm{jet}} > 10$ GeV threshold,

$$\sigma(\mathrm{Z+jet}) = 16.0 \pm 0.2\,(\mathrm{stat.}) \pm 1.2\,(\mathrm{syst.}) \pm 0.6\,(\mathrm{lumi.})\ \mathrm{pb},$$

$$\frac{\sigma(\mathrm{Z+jet})}{\sigma(\mathrm{Z})} = 0.209 \pm 0.002\,(\mathrm{stat.}) \pm 0.015\,(\mathrm{syst.}),$$

where the first uncertainty is statistical, the second is systematic and the third is the uncertainty due to the luminosity determination.

The measured cross-sections are compared to theoretical predictions at $\mathcal{O}(\alpha_s^2)$ calculated using POWHEG[15, 38–40]. The parton shower development and hadronisation are simulated using PYTHIA 6.4 [23], with the Perugia 0 tune [41]. Jets are created out of all stable particles in the final state that are not produced by the decay of the Z boson. These

predictions are computed with the renormalisation scale and factorisation scales set to the nominal value of the vector boson transverse momentum.

The theoretical predictions are computed for three different NLO PDF parametrisations: MSTW08 [42], CTEQ10 [43] and NNPDF 2.3 [44]. For the differential distributions, the CTEQ10 and NNPDF 2.3 results are calculated at $\mathcal{O}(\alpha_s^2)$. Results using the MSTW08 parametrisation are calculated at $\mathcal{O}(\alpha_s)$ and $\mathcal{O}(\alpha_s^2)$. For the ratio $\sigma_{\text{Z+jet}}/\sigma_{\text{Z}}$, the Z+jet cross-section is computed at $\mathcal{O}(\alpha_s^2)$ and the Z cross-section at $\mathcal{O}(\alpha_s)$ for the MSTW08, CTEQ10 and NNPDF 2.3 PDF parametrisations. To see the effect of higher orders in pQCD on the Z+jet cross-section, theoretical predictions are also computed by taking the ratio between the Z and Z+jet cross-sections at $\mathcal{O}(\alpha_s)$, with the PDFs determined from the MSTW08 NLO parametrisation.

In addition, the Z+jet cross-section is computed using FEWZ [13] at $\mathcal{O}(\alpha_s^2)$, with the MSTW08 NLO PDF parametrisation. The cross-section for inclusive Z boson production is calculated using FEWZ at $\mathcal{O}(\alpha_s)$, with the same PDF parametrisation. This theoretical prediction neglects effects from hadronisation and the underlying event, and so comparisons with the results and the other predictions are indicative of the size of these effects. For these calculations the renormalisation scale and factorisation scales are set to the nominal value of the vector boson mass.

Uncertainties on all predictions are calculated by repeating the calculations with the renormalisation and factorisation scales simultaneously varied by a factor of two about their nominal values. The spread in predictions from the different PDF parametrisations is indicative of the PDF uncertainty.

The cross-section ratios are compared in figure 3 to the Standard Model theoretical predictions discussed above. The results for the differential cross-sections, uncorrected for final state radiation from the muons, are presented in figures 4–9. For all cases reasonable agreement is seen between the Standard Model calculations and the data. The $\mathcal{O}(\alpha_s^2)$ predictions tend to give better agreement with data than the $\mathcal{O}(\alpha_s)$ prediction. This is most noticeably seen in the Z boson transverse momentum distribution, shown in figure 7. For high values of the boson transverse momentum, the $\mathcal{O}(\alpha_s^2)$ predictions have a slope compatible with that in data, whereas the $\mathcal{O}(\alpha_s)$ prediction is steeper than data. The $\mathcal{O}(\alpha_s^2)$ predictions also match the data better for the $\Delta\phi$ distribution, as shown in figure 8. The $\mathcal{O}(\alpha_s)$ prediction overestimates the number of events where the Z boson and jet are azimuthally opposed. Higher orders in pQCD are needed to simulate the production of Z bosons and jets that are not produced back-to-back as the parton shower tends to produce partons collinear with the parton produced in the hard interaction. Whilst the different PDF parametrisations studied agree with the data, there are hints of tension between the PDF sets in the Δy distribution, shown in figure 9.

8 Summary

A measurement of the $pp \to \text{Z}(\to \mu^+\mu^-) + \text{jet}$ production cross-section at $\sqrt{s} = 7\,\text{TeV}$ is presented, using a data sample corresponding to an integrated luminosity of $1.0\,\text{fb}^{-1}$ recorded by the LHCb experiment. The measurement is performed within the kinematic
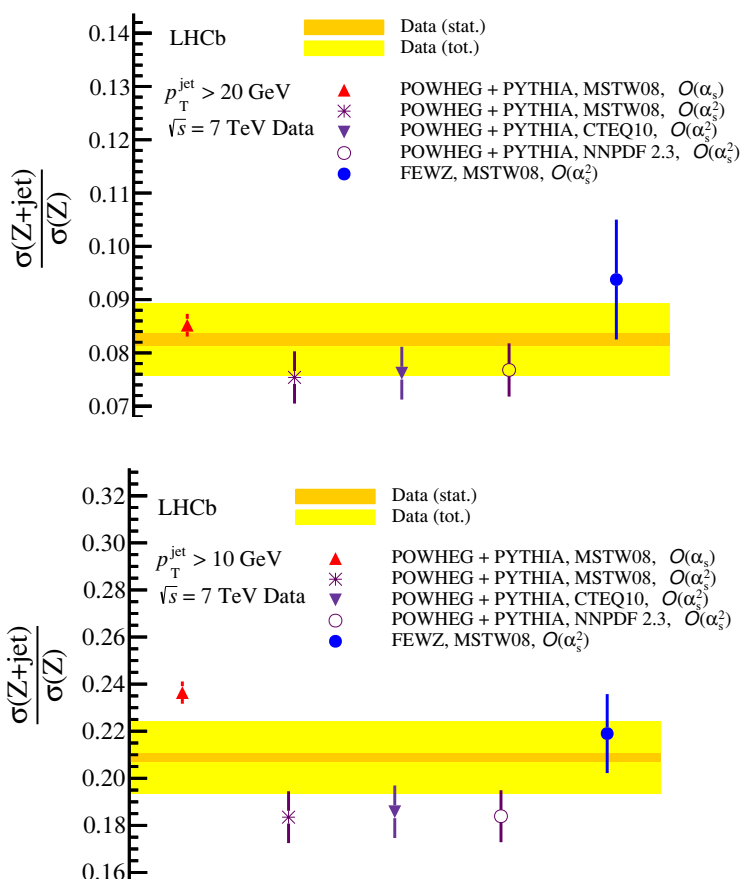
Figure 3. Ratio of the Z+jet cross-section to the inclusive cross-section, for (top) $p_{\rm T}^{\rm jet} > 20$ GeV and (bottom) $p_{\rm T}^{\rm jet} > 10$ GeV. The bands show the LHCb measurement (with the inner band showing the statistical uncertainty and the outer band showing the total uncertainty). The points correspond to different theoretical predictions with the error bars indicating their uncertainties as described in the main text. These results are corrected for FSR from the final state muons from the Z boson decay.

acceptance, $p_{\rm T}^{\mu} > 20$ GeV, $2.0 < \eta^{\mu} < 4.5$, $60 < M_{\mu\mu} < 120$ GeV, $2.0 < \eta^{\rm jet} < 4.5$ and $\Delta r(\mu, {\rm jet}) > 0.4$. The cross-sections are determined for jets with transverse momenta exceeding two thresholds, 20 and 10 GeV. The differential cross-sections are also measured as a function of various variables describing the Z boson kinematic properties, the jet kinematic properties, and the correlations between them. The measured cross-sections show reasonable agreement with expectations from $\mathcal{O}(\alpha_s^2)$ calculations, for all the PDF parametrisations studied. Predictions at $\mathcal{O}(\alpha_s^2)$ show better agreement with the $p_{\rm T}$ and $\Delta\phi$ distributions, which are sensitive to higher order effects, than predictions at $\mathcal{O}(\alpha_s)$.
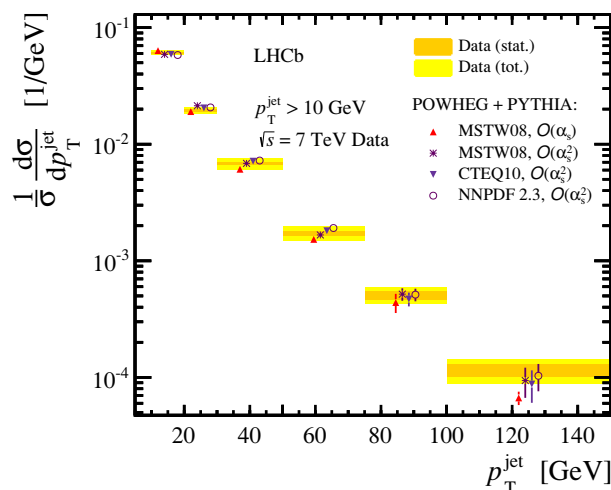
Acknowledgments

Figure 4. Cross-section for Z+jet production, differential in the leading jet p_T, for $p_T^{jet} > 10$ GeV. The bands show the LHCb measurement (with the inner band showing the statistical uncertainty and the outer band showing the total uncertainty). The points correspond to different theoretical predictions with the error bars indicating their uncertainties as described in the main text. Predictions are displaced horizontally for presentation. These results are not corrected for FSR from the final state muons from the Z boson decay.
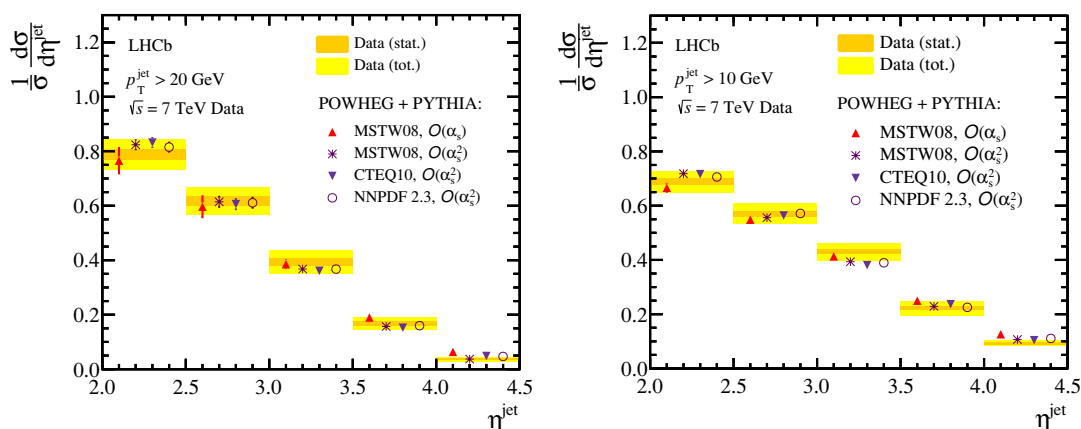

Figure 5. Cross-section for Z+jet production, differential in the leading jet pseudorapidity, for (left) $p_T^{jet} > 20$ GeV and (right) $p_T^{jet} > 10$ GeV. The bands show the LHCb measurement (with the inner band showing the statistical uncertainty and the outer band showing the total uncertainty). Superimposed are predictions as described in figure 4.
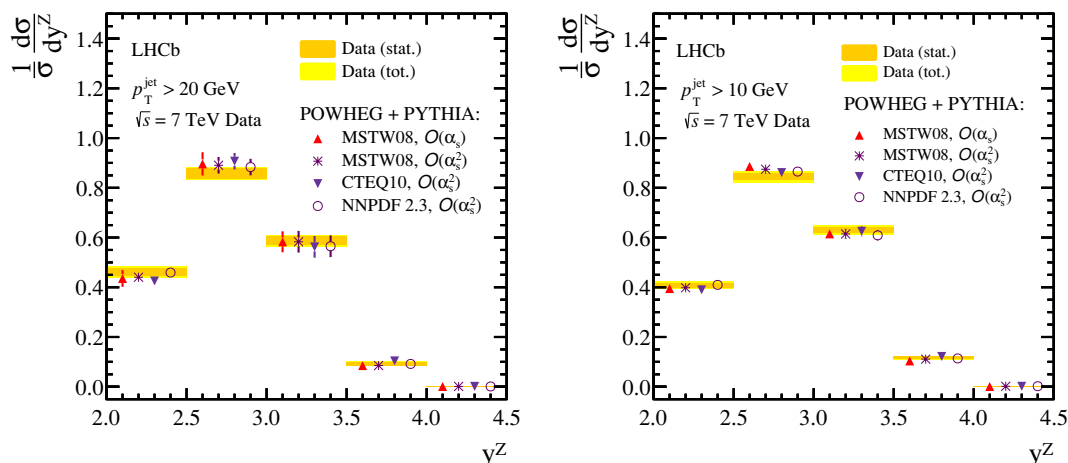
Figure 6. Cross-section for Z+jet production, differential in the Z boson rapidity, y^Z, for (left) $p_T^{jet} > 20$ GeV and (right) $p_T^{jet} > 10$ GeV. The bands show the LHCb measurement (with the inner band showing the statistical uncertainty and the outer band showing the total uncertainty). Superimposed are predictions as described in figure 4.

Figure 7. Cross-section for Z+jet production, differential in the Z boson transverse momentum, for (left) $p_T^{jet} > 20$ GeV and (right) $p_T^{jet} > 10$ GeV. The bands show the LHCb measurement (with the inner band showing the statistical uncertainty and the outer band showing the total uncertainty). Superimposed are predictions as described in figure 4.

Figure 8. Cross-section for Z+jet production, differential in the difference in ϕ between the Z boson and the leading jet, for (left) $p_T^{\text{jet}} > 20$ GeV and (right) $p_T^{\text{jet}} > 10$ GeV. The bands show the LHCb measurement (with the inner band showing the statistical uncertainty and the outer band showing the total uncertainty). Superimposed are predictions as described in figure 4.
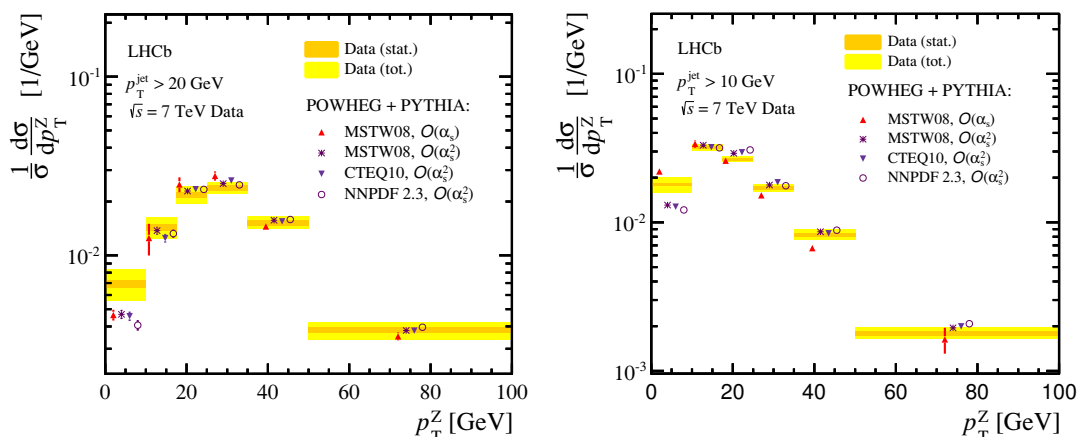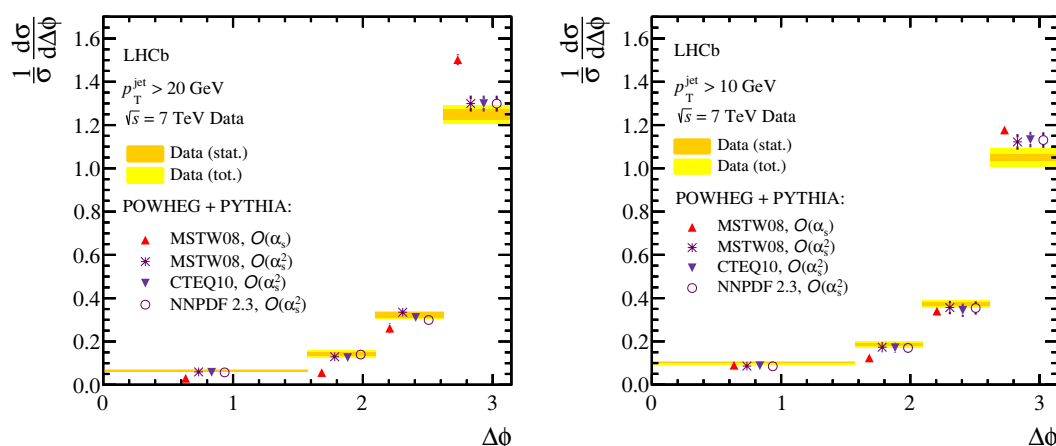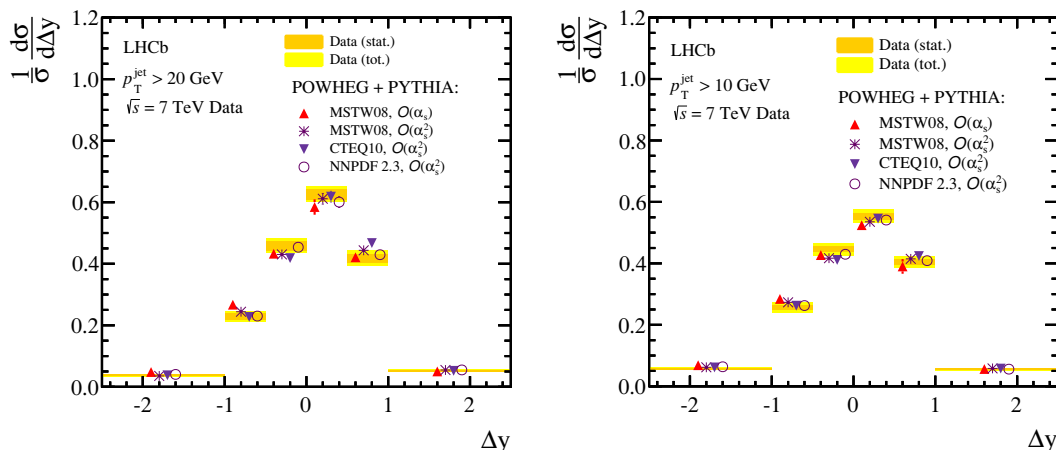

Figure 9. Cross-section for Z+jet production, differential in the difference in rapidity between the Z boson and the leading jet, for (left) $p_T^{\text{jet}} > 20$ GeV and (right) $p_T^{\text{jet}} > 10$ GeV. The bands show the LHCb measurement (with the inner band showing the statistical uncertainty and the outer band showing the total uncertainty). Superimposed are predictions as described in figure 4.

References

[1] R. Thorne, A. Martin, W. Stirling and G. Watt, *Parton distributions and QCD at LHCb*, arXiv:0808.1847 [INSPIRE].

[2] LHCb collaboration, *Inclusive W and Z production in the forward region at $\sqrt{s} = 7$ TeV*, *JHEP* **06** (2012) 058 [arXiv:1204.1620] [INSPIRE].

[3] LHCb collaboration, *Measurement of the cross-section for $Z \to e^+e^-$ production in pp collisions at $\sqrt{s} = 7$ TeV*, *JHEP* **02** (2013) 106 [arXiv:1212.4620] [INSPIRE].

[4] LHCb collaboration, *A study of the Z production cross-section in pp collisions at $\sqrt{s} = 7$ TeV using tau final states*, *JHEP* **01** (2013) 111 [arXiv:1210.6289] [INSPIRE].

[5] S.A. Malik and G. Watt, *Ratios of W and Z cross sections at large boson p_T as a constraint on PDFs and background to new physics*, `arXiv:1304.2424` [ɪɴSPIRE].

[6] ATLAS collaboration, *Measurement of the production cross section of jets in association with a Z boson in pp collisions at $\sqrt{s} = 7$ TeV with the ATLAS detector*, *JHEP* **07** (2013) 032 [`arXiv:1304.7098`] [ɪɴSPIRE].

[7] CMS collaboration, *Event shapes and azimuthal correlations in Z + jets events in pp collisions at $\sqrt{s} = 7$ TeV*, *Phys. Lett.* **B 722** (2013) 238 [`arXiv:1301.1646`] [ɪɴSPIRE].

[8] CMS collaboration, *Rapidity distributions in exclusive Z + jet and photon + jet events in pp collisions at $\sqrt{s} = 7$ TeV*, `arXiv:1310.3082` [ɪɴSPIRE].

[9] F. Hautmann, M. Hentschinski and H. Jung, *Forward Z-boson production and the unintegrated sea quark density*, *Nucl. Phys.* **B 865** (2012) 54 [`arXiv:1205.1759`] [ɪɴSPIRE].

[10] P.B. Arnold and M.H. Reno, *The complete computation of high p_T W and Z production in 2nd order QCD*, *Nucl. Phys.* **B 319** (1989) 37 [*Erratum ibid.* **B 330** (1990) 284] [ɪɴSPIRE].

[11] W. Giele, E.N. Glover and D.A. Kosower, *Higher order corrections to jet cross-sections in hadron colliders*, *Nucl. Phys.* **B 403** (1993) 633 [`hep-ph/9302225`] [ɪɴSPIRE].

[12] C. Anastasiou, L.J. Dixon, K. Melnikov and F. Petriello, *High precision QCD at hadron colliders: electroweak gauge boson rapidity distributions at NNLO*, *Phys. Rev.* **D 69** (2004) 094008 [`hep-ph/0312266`] [ɪɴSPIRE].

[13] R. Gavin, Y. Li, F. Petriello and S. Quackenbush, *FEWZ 2.0: a code for hadronic Z production at next-to-next-to-leading order*, *Comput. Phys. Commun.* **182** (2011) 2388 [`arXiv:1011.3540`] [ɪɴSPIRE].

[14] J.M. Campbell and R. Ellis, *MCFM for the Tevatron and the LHC*, *Nucl. Phys. Proc. Suppl.* **205-206** (2010) 10 [`arXiv:1007.3492`] [ɪɴSPIRE].

[15] S. Alioli, P. Nason, C. Oleari and E. Re, *Vector boson plus one jet production in POWHEG*, *JHEP* **01** (2011) 095 [`arXiv:1009.5594`] [ɪɴSPIRE].

[16] M.L. Mangano, M. Moretti, F. Piccinini, R. Pittau and A.D. Polosa, *ALPGEN, a generator for hard multiparton processes in hadronic collisions*, *JHEP* **07** (2003) 001 [`hep-ph/0206293`] [ɪɴSPIRE].

[17] T. Gleisberg et al., *Event generation with SHERPA 1.1*, *JHEP* **02** (2009) 007 [`arXiv:0811.4622`] [ɪɴSPIRE].

[18] M. Cacciari, G.P. Salam and G. Soyez, *The anti-k_t jet clustering algorithm*, *JHEP* **04** (2008) 063 [`arXiv:0802.1189`] [ɪɴSPIRE].

[19] LHCb collaboration, *The LHCb detector at the LHC*, 2008 *JINST* **3** S08005 [ɪɴSPIRE].

[20] M. Adinolfi et al., *Performance of the LHCb RICH detector at the LHC*, *Eur. Phys. J.* **C 73** (2013) 2431 [`arXiv:1211.6759`] [ɪɴSPIRE].

[21] J. Alves Jr. et al., *Performance of the LHCb muon system*, 2013 *JINST* **8** P02022 [`arXiv:1211.1346`] [ɪɴSPIRE].

[22] R. Aaij et al., *The LHCb trigger and its performance in 2011*, 2013 *JINST* **8** P04022 [`arXiv:1211.3055`] [ɪɴSPIRE].

[23] T. Sjöstrand, S. Mrenna and P.Z. Skands, *PYTHIA 6.4 physics and manual*, *JHEP* **05** (2006) 026 [`hep-ph/0603175`] [ɪɴSPIRE].

[24] I. Belyaev et al., *Handling of the generation of primary events in* Gauss*, the LHCb simulation framework*, *IEEE Nucl Sci. Symp. Conf. Rec.* (2010) 1155.

[25] P.M. Nadolsky et al., *Implications of CTEQ global analysis for collider observables*, *Phys. Rev.* **D 78** (2008) 013004 [arXiv:0802.0007] [INSPIRE].

[26] D. Lange, *The EvtGen particle decay simulation package*, *Nucl. Instrum. Meth.* **A 462** (2001) 152 [INSPIRE].

[27] P. Golonka and Z. Was, *PHOTOS Monte Carlo: a precision tool for QED corrections in Z and W decays*, *Eur. Phys. J.* **C 45** (2006) 97 [hep-ph/0506026] [INSPIRE].

[28] GEANT4 collaboration, J. Allison et al., *GEANT4 developments and applications*, *IEEE Trans. Nucl. Sci.* **53** (2006) 270.

[29] GEANT4 collaboration, S. Agostinelli et al., *GEANT4: a simulation toolkit*, *Nucl. Instrum. Meth.* **A 506** (2003) 250 [INSPIRE].

[30] M. Clemencic et al., *The LHCb simulation application, Gauss: design, evolution and experience*, *J. Phys. Conf. Ser.* **331** (2011) 032023 [INSPIRE].

[31] M. Cacciari and G.P. Salam, *Dispelling the N^3 myth for the k_t jet-finder*, *Phys. Lett.* **B 641** (2006) 57 [hep-ph/0512210] [INSPIRE].

[32] A. Jaeger et al., *Measurement of the track finding efficiency*, LHCb-PUB-2011-025 (2011).

[33] G. D'Agostini, *A multidimensional unfolding method based on Bayes' theorem*, *Nucl. Instrum. Meth.* **A 362** (1995) 487 [INSPIRE].

[34] T. Adye, *Unfolding algorithms and tests using RooUnfold*, in *PHYSTAT 2011 Workshop on Statistical Issues Related to Discovery Claims in Search Experiments and Unfolding*, January 17–20, CERN, Geneva, Switzerland (2011), arXiv:1105.1160 [INSPIRE].

[35] A. Hocker and V. Kartvelishvili, *SVD approach to data unfolding*, *Nucl. Instrum. Meth.* **A 372** (1996) 469 [hep-ph/9509307] [INSPIRE].

[36] LHCb collaboration, R. Aaij et al., *Absolute luminosity measurements with the LHCb detector at the LHC*, 2012 *JINST* **7** P01010 [arXiv:1110.2866] [INSPIRE].

[37] M. Bahr et al., *HERWIG++ physics and manual*, *Eur. Phys. J.* **C 58** (2008) 639 [arXiv:0803.0883] [INSPIRE].

[38] P. Nason, *A New method for combining NLO QCD with shower Monte Carlo algorithms*, *JHEP* **11** (2004) 040 [hep-ph/0409146] [INSPIRE].

[39] S. Frixione, P. Nason and C. Oleari, *Matching NLO QCD computations with parton shower simulations: the POWHEG method*, *JHEP* **11** (2007) 070 [arXiv:0709.2092] [INSPIRE].

[40] S. Alioli, P. Nason, C. Oleari and E. Re, *A general framework for implementing NLO calculations in shower Monte Carlo programs: the POWHEG BOX*, *JHEP* **06** (2010) 043 [arXiv:1002.2581] [INSPIRE].

[41] P.Z. Skands, *Tuning Monte Carlo generators: the Perugia tunes*, *Phys. Rev.* **D 82** (2010) 074018 [arXiv:1005.3457] [INSPIRE].

[42] A. Martin, W. Stirling, R. Thorne and G. Watt, *Parton distributions for the LHC*, *Eur. Phys. J.* **C 63** (2009) 189 [arXiv:0901.0002] [INSPIRE].

[43] H.-L. Lai et al., *New parton distributions for collider physics*, *Phys. Rev.* **D 82** (2010) 074024 [arXiv:1007.2241] [INSPIRE].

[44] R.D. Ball et al., *Parton distributions with LHC data*, *Nucl. Phys.* **B 867** (2013) 244 [arXiv:1207.1303] [INSPIRE].

The LHCb collaboration

R. Aaij[40], B. Adeva[36], M. Adinolfi[45], C. Adrover[6], A. Affolder[51], Z. Ajaltouni[5], J. Albrecht[9],
F. Alessio[37], M. Alexander[50], S. Ali[40], G. Alkhazov[29], P. Alvarez Cartelle[36], A.A. Alves Jr[24],
S. Amato[2], S. Amerio[21], Y. Amhis[7], L. Anderlini[17,f], J. Anderson[39], R. Andreassen[56],
M. Andreotti[16,e], J.E. Andrews[57], R.B. Appleby[53], O. Aquines Gutierrez[10], F. Archilli[37],
A. Artamonov[34], M. Artuso[58], E. Aslanides[6], G. Auriemma[24,m], M. Baalouch[5], S. Bachmann[11],
J.J. Back[47], A. Badalov[35], C. Baesso[59], V. Balagura[30], W. Baldini[16], R.J. Barlow[53],
C. Barschel[37], S. Barsuk[7], W. Barter[46], V. Batozskaya[27], Th. Bauer[40], A. Bay[38], J. Beddow[50],
F. Bedeschi[22], I. Bediaga[1], S. Belogurov[30], K. Belous[34], I. Belyaev[30], E. Ben-Haim[8],
G. Bencivenni[18], S. Benson[49], J. Benton[45], A. Berezhnoy[31], R. Bernet[39], M.-O. Bettler[46],
M. van Beuzekom[40], A. Bien[11], S. Bifani[44], T. Bird[53], A. Bizzeti[17,h], P.M. Bjørnstad[53],
T. Blake[47], F. Blanc[38], J. Blouw[10], S. Blusk[58], V. Bocci[24], A. Bondar[33], N. Bondar[29],
W. Bonivento[15,37], S. Borghi[53], A. Borgia[58], T.J.V. Bowcock[51], E. Bowen[39], C. Bozzi[16],
T. Brambach[9], J. van den Brand[41], J. Bressieux[38], D. Brett[53], M. Britsch[10], T. Britton[58],
N.H. Brook[45], H. Brown[51], A. Bursche[39], G. Busetto[21,q], J. Buytaert[37], S. Cadeddu[15],
R. Calabrese[16,e], O. Callot[7], M. Calvi[20,j], M. Calvo Gomez[35,n], A. Camboni[35], P. Campana[18,37],
D. Campora Perez[37], A. Carbone[14,c], G. Carboni[23,k], R. Cardinale[19,i], A. Cardini[15],
H. Carranza-Mejia[49], L. Carson[52], K. Carvalho Akiba[2], G. Casse[51], L. Castillo Garcia[37],
M. Cattaneo[37], Ch. Cauet[9], R. Cenci[57], M. Charles[8], Ph. Charpentier[37], S.-F. Cheung[54],
N. Chiapolini[39], M. Chrzaszcz[39,25], K. Ciba[37], X. Cid Vidal[37], G. Ciezarek[52], P.E.L. Clarke[49],
M. Clemencic[37], H.V. Cliff[46], J. Closier[37], C. Coca[28], V. Coco[40], J. Cogan[6], E. Cogneras[5],
P. Collins[37], A. Comerma-Montells[35], A. Contu[15,37], A. Cook[45], M. Coombes[45], S. Coquereau[8],
G. Corti[37], B. Couturier[37], G.A. Cowan[49], D.C. Craik[47], M. Cruz Torres[59], S. Cunliffe[52],
R. Currie[49], C. D'Ambrosio[37], J. Dalseno[45], P. David[8], P.N.Y. David[40], A. Davis[56], I. De Bonis[4],
K. De Bruyn[40], S. De Capua[53], M. De Cian[11], J.M. De Miranda[1], L. De Paula[2], W. De Silva[56],
P. De Simone[18], D. Decamp[4], M. Deckenhoff[9], L. Del Buono[8], N. Déléage[4], D. Derkach[54],
O. Deschamps[5], F. Dettori[41], A. Di Canto[11], H. Dijkstra[37], M. Dogaru[28], S. Donleavy[51],
F. Dordei[11], A. Dosil Suárez[36], D. Dossett[47], A. Dovbnya[42], F. Dupertuis[38], P. Durante[37],
R. Dzhelyadin[34], A. Dziurda[25], A. Dzyuba[29], S. Easo[48], U. Egede[52], V. Egorychev[30],
S. Eidelman[33], D. van Eijk[40], S. Eisenhardt[49], U. Eitschberger[9], R. Ekelhof[9], L. Eklund[50,37],
I. El Rifai[5], Ch. Elsasser[39], A. Falabella[14,e], C. Färber[11], C. Farinelli[40], S. Farry[51], D. Ferguson[49],
V. Fernandez Albor[36], F. Ferreira Rodrigues[1], M. Ferro-Luzzi[37], S. Filippov[32], M. Fiore[16,e],
M. Fiorini[16,e], C. Fitzpatrick[37], M. Fontana[10], F. Fontanelli[19,i], R. Forty[37], O. Francisco[2],
M. Frank[37], C. Frei[37], M. Frosini[17,37,f], E. Furfaro[23,k], A. Gallas Torreira[36], D. Galli[14,c],
M. Gandelman[2], P. Gandini[58], Y. Gao[3], J. Garofoli[58], P. Garosi[53], J. Garra Tico[46], L. Garrido[35],
C. Gaspar[37], R. Gauld[54], E. Gersabeck[11], M. Gersabeck[53], T. Gershon[47], Ph. Ghez[4], V. Gibson[46],
L. Giubega[28], V.V. Gligorov[37], C. Göbel[59], D. Golubkov[30], A. Golutvin[52,30,37], A. Gomes[2],
P. Gorbounov[30,37], H. Gordon[37], M. Grabalosa Gándara[5], R. Graciani Diaz[35],
L.A. Granado Cardoso[37], E. Graugés[35], G. Graziani[17], A. Grecu[28], E. Greening[54], S. Gregson[46],
P. Griffith[44], L. Grillo[11], O. Grünberg[60], B. Gui[58], E. Gushchin[32], Yu. Guz[34,37], T. Gys[37],
C. Hadjivasiliou[58], G. Haefeli[38], C. Haen[37], T.W. Hafkenscheid[61], S.C. Haines[46], S. Hall[52],
B. Hamilton[57], T. Hampson[45], S. Hansmann-Menzemer[11], N. Harnew[54], S.T. Harnew[45],
J. Harrison[53], T. Hartmann[60], J. He[37], T. Head[37], V. Heijne[40], K. Hennessy[51], P. Henrard[5],
J.A. Hernando Morata[36], E. van Herwijnen[37], M. Heß[60], A. Hicheur[1], E. Hicks[51], D. Hill[54],
M. Hoballah[5], C. Hombach[53], W. Hulsbergen[40], P. Hunt[54], T. Huse[51], N. Hussain[54],
D. Hutchcroft[51], D. Hynds[50], V. Iakovenko[43], M. Idzik[26], P. Ilten[12], R. Jacobsson[37], A. Jaeger[11],
E. Jans[40], P. Jaton[38], A. Jawahery[57], F. Jing[3], M. John[54], D. Johnson[54], C.R. Jones[46],

C. Joram[37], B. Jost[37], M. Kaballo[9], S. Kandybei[42], W. Kanso[6], M. Karacson[37], T.M. Karbach[37],
I.R. Kenyon[44], T. Ketel[41], B. Khanji[20], S. Klaver[53], O. Kochebina[7], I. Komarov[38],
R.F. Koopman[41], P. Koppenburg[40], M. Korolev[31], A. Kozlinskiy[40], L. Kravchuk[32], K. Kreplin[11],
M. Kreps[47], G. Krocker[11], P. Krokovny[33], F. Kruse[9], M. Kucharczyk[20,25,37,j], V. Kudryavtsev[33],
K. Kurek[27], T. Kvaratskheliya[30,37], V.N. La Thi[38], D. Lacarrere[37], G. Lafferty[53], A. Lai[15],
D. Lambert[49], R.W. Lambert[41], E. Lanciotti[37], G. Lanfranchi[18], C. Langenbruch[37], T. Latham[47],
C. Lazzeroni[44], R. Le Gac[6], J. van Leerdam[40], J.-P. Lees[4], R. Lefèvre[5], A. Leflat[31], J. Lefrançois[7],
S. Leo[22], O. Leroy[6], T. Lesiak[25], B. Leverington[11], Y. Li[3], L. Li Gioi[5], M. Liles[51], R. Lindner[37],
C. Linn[11], B. Liu[3], G. Liu[37], S. Lohn[37], I. Longstaff[50], J.H. Lopes[2], N. Lopez-March[38], H. Lu[3],
D. Lucchesi[21,q], J. Luisier[38], H. Luo[49], E. Luppi[16,e], O. Lupton[54], F. Machefert[7],
I.V. Machikhiliyan[30], F. Maciuc[28], O. Maev[29,37], S. Malde[54], G. Manca[15,d], G. Mancinelli[6],
J. Maratas[5], U. Marconi[14], P. Marino[22,s], R. Märki[38], J. Marks[11], G. Martellotti[24], A. Martens[8],
A. Martín Sánchez[7], M. Martinelli[40], D. Martinez Santos[41,37], D. Martins Tostes[2], A. Martynov[31],
A. Massafferri[1], R. Matev[37], Z. Mathe[37], C. Matteuzzi[20], E. Maurice[6], A. Mazurov[16,37,e],
M. McCann[52], J. McCarthy[44], A. McNab[53], R. McNulty[12], B. McSkelly[51], B. Meadows[56,54],
F. Meier[9], M. Meissner[11], M. Merk[40], D.A. Milanes[8], M.-N. Minard[4], J. Molina Rodriguez[59],
S. Monteil[5], D. Moran[53], P. Morawski[25], A. Mordà[6], M.J. Morello[22,s], R. Mountain[58], I. Mous[40],
F. Muheim[49], K. Müller[39], R. Muresan[28], B. Muryn[26], B. Muster[38], P. Naik[45], T. Nakada[38],
R. Nandakumar[48], I. Nasteva[1], M. Needham[49], S. Neubert[37], N. Neufeld[37], A.D. Nguyen[38],
T.D. Nguyen[38], C. Nguyen-Mau[38,o], M. Nicol[7], V. Niess[5], R. Niet[9], N. Nikitin[31], T. Nikodem[11],
A. Nomerotski[54], A. Novoselov[34], A. Oblakowska-Mucha[26], V. Obraztsov[34], S. Oggero[40],
S. Ogilvy[50], O. Okhrimenko[43], R. Oldeman[15,d], G. Onderwater[61], M. Orlandea[28],
J.M. Otalora Goicochea[2], P. Owen[52], A. Oyanguren[35], B.K. Pal[58], A. Palano[13,b], M. Palutan[18],
J. Panman[37], A. Papanestis[48,37], M. Pappagallo[50], C. Parkes[53], C.J. Parkinson[52], G. Passaleva[17],
G.D. Patel[51], M. Patel[52], C. Patrignani[19,i], C. Pavel-Nicorescu[28], A. Pazos Alvarez[36],
A. Pearce[53], A. Pellegrino[40], G. Penso[24,l], M. Pepe Altarelli[37], S. Perazzini[14,c], E. Perez Trigo[36],
A. Pérez-Calero Yzquierdo[35], P. Perret[5], M. Perrin-Terrin[6], L. Pescatore[44], E. Pesen[62],
G. Pessina[20], K. Petridis[52], A. Petrolini[19,i], E. Picatoste Olloqui[35], B. Pietrzyk[4], T. Pilař[47],
D. Pinci[24], S. Playfer[49], M. Plo Casasus[36], F. Polci[8], G. Polok[25], A. Poluektov[47,33], E. Polycarpo[2],
A. Popov[34], D. Popov[10], B. Popovici[28], C. Potterat[35], A. Powell[54], J. Prisciandaro[38],
A. Pritchard[51], C. Prouve[7], V. Pugatch[43], A. Puig Navarro[38], G. Punzi[22,r], W. Qian[4],
B. Rachwal[25], J.H. Rademacker[45], B. Rakotomiaramanana[38], M.S. Rangel[2], I. Raniuk[42],
N. Rauschmayr[37], G. Raven[41], S. Redford[54], S. Reichert[53], M.M. Reid[47], A.C. dos Reis[1],
S. Ricciardi[48], A. Richards[52], K. Rinnert[51], V. Rives Molina[35], D.A. Roa Romero[5], P. Robbe[7],
D.A. Roberts[57], A.B. Rodrigues[1], E. Rodrigues[53], P. Rodriguez Perez[36], S. Roiser[37],
V. Romanovsky[34], A. Romero Vidal[36], M. Rotondo[21], J. Rouvinet[38], T. Ruf[37], F. Ruffini[22],
H. Ruiz[35], P. Ruiz Valls[35], G. Sabatino[24,k], J.J. Saborido Silva[36], N. Sagidova[29], P. Sail[50],
B. Saitta[15,d], V. Salustino Guimaraes[2], B. Sanmartin Sedes[36], R. Santacesaria[24],
C. Santamarina Rios[36], E. Santovetti[23,k], M. Sapunov[6], A. Sarti[18], C. Satriano[24,m], A. Satta[23],
M. Savrie[16,e], D. Savrina[30,31], M. Schiller[41], H. Schindler[37], M. Schlupp[9], M. Schmelling[10],
B. Schmidt[37], O. Schneider[38], A. Schopper[37], M.-H. Schune[7], R. Schwemmer[37], B. Sciascia[18],
A. Sciubba[24], M. Seco[36], A. Semennikov[30], K. Senderowska[26], I. Sepp[52], N. Serra[39], J. Serrano[6],
P. Seyfert[11], M. Shapkin[34], I. Shapoval[16,42,e], Y. Shcheglov[29], T. Shears[51], L. Shekhtman[33],
O. Shevchenko[42], V. Shevchenko[30], A. Shires[9], R. Silva Coutinho[47], M. Sirendi[46], N. Skidmore[45],
T. Skwarnicki[58], N.A. Smith[51], E. Smith[54,48], E. Smith[52], J. Smith[46], M. Smith[53],
M.D. Sokoloff[56], F.J.P. Soler[50], F. Soomro[38], D. Souza[45], B. Souza De Paula[2], B. Spaan[9],
A. Sparkes[49], P. Spradlin[50], F. Stagni[37], S. Stahl[11], O. Steinkamp[39], S. Stevenson[54], S. Stoica[28],
S. Stone[58], B. Storaci[39], S. Stracka[22,37], M. Straticiuc[28], U. Straumann[39], V.K. Subbiah[37],

L. Sun[56], W. Sutcliffe[52], S. Swientek[9], V. Syropoulos[41], M. Szczekowski[27], P. Szczypka[38,37],
D. Szilard[2], T. Szumlak[26], S. T'Jampens[4], M. Teklishyn[7], G. Tellarini[16,e], E. Teodorescu[28],
F. Teubert[37], C. Thomas[54], E. Thomas[37], J. van Tilburg[11], V. Tisserand[4], M. Tobin[38], S. Tolk[41],
L. Tomassetti[16,e], D. Tonelli[37], S. Topp-Joergensen[54], N. Torr[54], E. Tournefier[4,52], S. Tourneur[38],
M.T. Tran[38], M. Tresch[39], A. Tsaregorodtsev[6], P. Tsopelas[40], N. Tuning[40,37], M. Ubeda Garcia[37],
A. Ukleja[27], A. Ustyuzhanin[52,p], U. Uwer[11], V. Vagnoni[14], G. Valenti[14], A. Vallier[7],
R. Vazquez Gomez[18], P. Vazquez Regueiro[36], C. Vázquez Sierra[36], S. Vecchi[16], J.J. Velthuis[45],
M. Veltri[17,g], G. Veneziano[38], M. Vesterinen[37], B. Viaud[7], D. Vieira[2], X. Vilasis-Cardona[35,n],
A. Vollhardt[39], D. Volyanskyy[10], D. Voong[45], A. Vorobyev[29], V. Vorobyev[33], C. Voß[60], H. Voss[10],
R. Waldi[60], C. Wallace[47], R. Wallace[12], S. Wandernoth[11], J. Wang[58], D.R. Ward[46],
N.K. Watson[44], A.D. Webber[53], D. Websdale[52], M. Whitehead[47], J. Wicht[37], J. Wiechczynski[25],
D. Wiedner[11], L. Wiggers[40], G. Wilkinson[54], M.P. Williams[47,48], M. Williams[55], F.F. Wilson[48],
J. Wimberley[57], J. Wishahi[9], W. Wislicki[27], M. Witek[25], G. Wormser[7], S.A. Wotton[46],
S. Wright[46], S. Wu[3], K. Wyllie[37], Y. Xie[49,37], Z. Xing[58], Z. Yang[3], X. Yuan[3], O. Yushchenko[34],
M. Zangoli[14], M. Zavertyaev[10,a], F. Zhang[3], L. Zhang[58], W.C. Zhang[12], Y. Zhang[3],
A. Zhelezov[11], A. Zhokhov[30], L. Zhong[3], A. Zvyagin[37]

1   Centro Brasileiro de Pesquisas Físicas (CBPF), Rio de Janeiro, Brazil
2   Universidade Federal do Rio de Janeiro (UFRJ), Rio de Janeiro, Brazil
3   Center for High Energy Physics, Tsinghua University, Beijing, China
4   LAPP, Université de Savoie, CNRS/IN2P3, Annecy-Le-Vieux, France
5   Clermont Université, Université Blaise Pascal, CNRS/IN2P3, LPC, Clermont-Ferrand, France
6   CPPM, Aix-Marseille Université, CNRS/IN2P3, Marseille, France
7   LAL, Université Paris-Sud, CNRS/IN2P3, Orsay, France
8   LPNHE, Université Pierre et Marie Curie, Université Paris Diderot, CNRS/IN2P3, Paris, France
9   Fakultät Physik, Technische Universität Dortmund, Dortmund, Germany
10 Max-Planck-Institut für Kernphysik (MPIK), Heidelberg, Germany
11 Physikalisches Institut, Ruprecht-Karls-Universität Heidelberg, Heidelberg, Germany
12 School of Physics, University College Dublin, Dublin, Ireland
13 Sezione INFN di Bari, Bari, Italy
14 Sezione INFN di Bologna, Bologna, Italy
15 Sezione INFN di Cagliari, Cagliari, Italy
16 Sezione INFN di Ferrara, Ferrara, Italy
17 Sezione INFN di Firenze, Firenze, Italy
18 Laboratori Nazionali dell'INFN di Frascati, Frascati, Italy
19 Sezione INFN di Genova, Genova, Italy
20 Sezione INFN di Milano Bicocca, Milano, Italy
21 Sezione INFN di Padova, Padova, Italy
22 Sezione INFN di Pisa, Pisa, Italy
23 Sezione INFN di Roma Tor Vergata, Roma, Italy
24 Sezione INFN di Roma La Sapienza, Roma, Italy
25 Henryk Niewodniczanski Institute of Nuclear Physics Polish Academy of Sciences, Kraków, Poland
26 AGH - University of Science and Technology, Faculty of Physics and Applied Computer Science, Kraków, Poland
27 National Center for Nuclear Research (NCBJ), Warsaw, Poland
28 Horia Hulubei National Institute of Physics and Nuclear Engineering, Bucharest-Magurele, Romania
29 Petersburg Nuclear Physics Institute (PNPI), Gatchina, Russia
30 Institute of Theoretical and Experimental Physics (ITEP), Moscow, Russia
31 Institute of Nuclear Physics, Moscow State University (SINP MSU), Moscow, Russia
32 Institute for Nuclear Research of the Russian Academy of Sciences (INR RAN), Moscow, Russia

[33] *Budker Institute of Nuclear Physics (SB RAS) and Novosibirsk State University, Novosibirsk, Russia*

[34] *Institute for High Energy Physics (IHEP), Protvino, Russia*

[35] *Universitat de Barcelona, Barcelona, Spain*

[36] *Universidad de Santiago de Compostela, Santiago de Compostela, Spain*

[37] *European Organization for Nuclear Research (CERN), Geneva, Switzerland*

[38] *Ecole Polytechnique Fédérale de Lausanne (EPFL), Lausanne, Switzerland*

[39] *Physik-Institut, Universität Zürich, Zürich, Switzerland*

[40] *Nikhef National Institute for Subatomic Physics, Amsterdam, The Netherlands*

[41] *Nikhef National Institute for Subatomic Physics and VU University Amsterdam, Amsterdam, The Netherlands*

[42] *NSC Kharkiv Institute of Physics and Technology (NSC KIPT), Kharkiv, Ukraine*

[43] *Institute for Nuclear Research of the National Academy of Sciences (KINR), Kyiv, Ukraine*

[44] *University of Birmingham, Birmingham, United Kingdom*

[45] *H.H. Wills Physics Laboratory, University of Bristol, Bristol, United Kingdom*

[46] *Cavendish Laboratory, University of Cambridge, Cambridge, United Kingdom*

[47] *Department of Physics, University of Warwick, Coventry, United Kingdom*

[48] *STFC Rutherford Appleton Laboratory, Didcot, United Kingdom*

[49] *School of Physics and Astronomy, University of Edinburgh, Edinburgh, United Kingdom*

[50] *School of Physics and Astronomy, University of Glasgow, Glasgow, United Kingdom*

[51] *Oliver Lodge Laboratory, University of Liverpool, Liverpool, United Kingdom*

[52] *Imperial College London, London, United Kingdom*

[53] *School of Physics and Astronomy, University of Manchester, Manchester, United Kingdom*

[54] *Department of Physics, University of Oxford, Oxford, United Kingdom*

[55] *Massachusetts Institute of Technology, Cambridge, MA, United States*

[56] *University of Cincinnati, Cincinnati, OH, United States*

[57] *University of Maryland, College Park, MD, United States*

[58] *Syracuse University, Syracuse, NY, United States*

[59] *Pontifícia Universidade Católica do Rio de Janeiro (PUC-Rio), Rio de Janeiro, Brazil, associated to [2]*

[60] *Institut für Physik, Universität Rostock, Rostock, Germany, associated to [11]*

[61] *KVI - University of Groningen, Groningen, The Netherlands, associated to [40]*

[62] *Celal Bayar University, Manisa, Turkey, associated to [37]*

[a] *P.N. Lebedev Physical Institute, Russian Academy of Science (LPI RAS), Moscow, Russia*

[b] *Università di Bari, Bari, Italy*

[c] *Università di Bologna, Bologna, Italy*

[d] *Università di Cagliari, Cagliari, Italy*

[e] *Università di Ferrara, Ferrara, Italy*

[f] *Università di Firenze, Firenze, Italy*

[g] *Università di Urbino, Urbino, Italy*

[h] *Università di Modena e Reggio Emilia, Modena, Italy*

[i] *Università di Genova, Genova, Italy*

[j] *Università di Milano Bicocca, Milano, Italy*

[k] *Università di Roma Tor Vergata, Roma, Italy*

[l] *Università di Roma La Sapienza, Roma, Italy*

[m] *Università della Basilicata, Potenza, Italy*

[n] *LIFAELS, La Salle, Universitat Ramon Llull, Barcelona, Spain*

[o] *Hanoi University of Science, Hanoi, Viet Nam*

[p] *Institute of Physics and Technology, Moscow, Russia*

[q] *Università di Padova, Padova, Italy*

[r] *Università di Pisa, Pisa, Italy*

[s] *Scuola Normale Superiore, Pisa, Italy*